Faraday Discussions

Accepted Manuscript

This manuscript will be presented and discussed at a forthcoming Faraday Discussion meeting. All delegates can contribute to the discussion which will be included in the final volume.

Register now to attend! Full details of all upcoming meetings: http://rsc.li/fd-upcoming-meetings

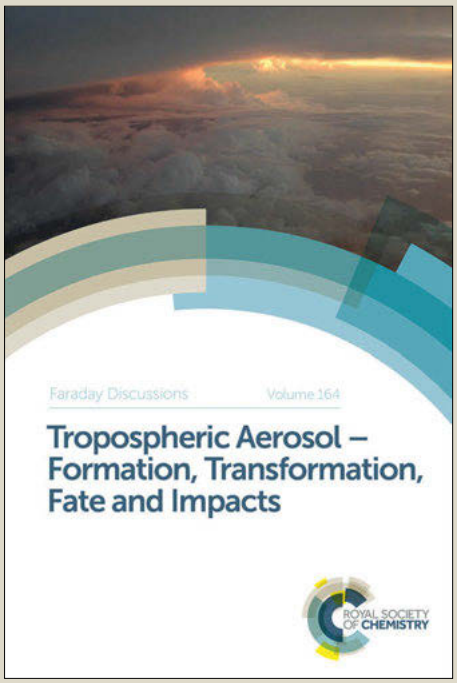

This is an *Accepted Manuscript*, which has been through the Royal Society of Chemistry peer review process and has been accepted for publication.

Accepted Manuscripts are published online shortly after acceptance, before technical editing, formatting and proof reading. Using this free service, authors can make their results available to the community, in citable form, before we publish the edited article. We will replace this *Accepted Manuscript* with the edited and formatted *Advance Article* as soon as it is available.

You can find more information about *Accepted Manuscripts* in the Information for Authors.

Please note that technical editing may introduce minor changes to the text and/or graphics, which may alter content. The journal's standard Terms & Conditions and the Ethical guidelines still apply. In no event shall the Royal Society of Chemistry be held responsible for any errors or omissions in this *Accepted Manuscript* or any consequences arising from the use of any information it contains.

ROYAL SOCIETY OF CHEMISTRY

www.rsc.org/faraday_d

CREATED USING THE RSC REPORT TEMPLATE (VER. 3.1) - SEE WWW.RSC.ORG/ELECTRONICFILES FOR DETAILS
Faraday Discussions
REVIEW www.rsc.org/xxxxxx | XXXXXXXX

Laser Heated Boron Doped Diamond Electrodes: Effect of Temperature on Outer Sphere Electron Transfer Processes

Lingcong Meng[a†], James G. Iacobini[a†], Maxim B. Joseph[a], Julie V. Macpherson[a*] and Mark E Newton[b*]

DOI: 10.1039/b000000x [DO NOT ALTER/DELETE THIS TEXT]

[†]Both authors contributed equally in this work

Thermoelectrochemical experiments can reveal significant information about electrochemical processes compared to ambient only measurements. Typical thermoelectrochemistry is performed using resistively heated wires or laser heated electrodes, both of which can suffer drawbacks associated with the electrode material employed. Boron doped diamond (BDD) is ideal for thermoelectrochemical investigations due to its extremely high thermal conductivity and diffusivity, extreme resistance to thermal ablation (can withstand laser power densities, P_d, of GW cm^{-2} for nanosecond pulses) and excellent electrochemical properties (low background currents and wide potential window). In this paper we describe the use of a pulsed laser technique to heat the rear of a 1 mm diameter conducting BDD disc electrode, which drives electrochemical solution reactions at the front face. Maximum average electrode temperatures of 90.0 ^{o}C were recorded experimentally and confirmed by finite element modelling (FEM). The effect of laser pulsed heating (maximum 3.8 kW cm^{-2}; 10 ms on and 90 ms off) on the cyclic voltammetric response of two fast (reversible) outer sphere electron transfer redox mediators ($Ru(NH_3)_6^{3+/2+}$ and $IrCl_6^{2-/3-}$) are investigated. In particular, we observe pulsed increases in the current, which increase with increasing P_d. The potential of the peak current is shifted positively for the $Ru(NH_3)_6^{3+/2+}$ couple (in accordance with a positive temperature coefficient, β, +0.68 mV K^{-1}) and negatively for the $IrCl_6^{3-/2-}$ couple (β = -0.48 mV K^{-1}). Scanning backwards, in contrast to that observed for a macrodisc electrode in ambient solution, a cathodic peak is again observed for $Ru(NH_3)_6^{3+/2+}$ and an anodic peak for $IrCl_6^{3-/2-}$ couple. We attribute this response to the entropy of the redox reaction and the time-dependant change in mass transport due to the induced thermal gradients at the electrode/electrolyte interface. The observed responses are in qualitative agreement with FEM simulations.

1 Introduction

The effect of temperature, T, in electrochemistry is of great importance[1, 2] yet most electrochemical experiments are performed under ambient conditions. This is surprising since T plays a key role in determining the thermodynamics and kinetics of electron transfer processes,[3, 4] affects adsorption/desorption processes and double layer phenomena and is intrinsically linked to the mass transport properties of the system. It is also often the case that model systems proposed for real processes operating at elevated temperatures e.g. oxygen reduction reaction associated with fuel cells, are carried out under ambient conditions.[5, 6]

Thermoelectrochemistry[7] is the branch of electrochemistry where temperature is a controlled variable in the electrochemical experiment. The simplest means of

controlling temperature is to use an isothermal approach, heating or cooling the system to the required temperature as appropriate. However, mass transport is often ill-defined due to uncontrolled thermal gradients in the solution, and systematically varying T is a slow process.[8] By moving to non-isothermal methodologies where heat is applied locally to the working electrode, a well-defined temperature gradient now exists at the electrode-electrolyte interface, meaning mass transport can be quantified in the system. It is also possible to heat and change the temperature much faster by utilising short thermal pulses. Finally, the temperature at the electrode/electrolyte interface can be driven above the boiling point. As the electrode only sits at these elevated temperatures for brief periods of time, bubbling is avoided.

Different approaches to non-isothermal heating have been adopted[3] although the most popular in the literature are Joule heating and laser heating. In the former, the electrode can either be heated directly or indirectly, although the direct approach gives rise to the fastest thermal changes and is most widely used. Here the electrode is typically heated via application of an alternating current or radio frequency waves.[3] Thermal modulation by laser heating was proposed in 1975 by Barker and Gardner.[9] Since then laser heating using a pulsed laser has become a popular method of choice.[10-14] The lasers employed typically range in power densities, P_d, (mW cm^{-2} - GW cm^{-2}), wavelength (355 nm - 1064 nm), and pulse width (~10's of ps – 10's of ms) and have been used to examine a variety of different temperature dependant electrochemical phenomena, ranging from electrode kinetics,[13, 14,15, 16] double layer structure elucidation[17] and surface cleaning.[10,18] Typically the laser is either focused onto the back face of the electrode[13, 14,18] or focused directly onto the front face, passing through solution[10,11,12,15] where energy will be lost, the amount dependant on the path length and absorption coefficient of solution. Local temperature increases typically vary from a few K to 500 K dependant on laser operation conditions.[12]

An important consideration in all thermoelectrochemical experiments is the geometrical arrangement and electrode material employed. Non-isothermal, Joule heated microwire electrodes have proven popular due to decreased Ohmic drop and higher rates of mass transport, compared to macroelectrodes.[3] In general, metal electrodes such as Pt and Au are employed due to their high electrical and thermal conductivities. However, the electrode materials have limitations. For example, it has been shown that even after mild laser treatments (P_d > 1.5 W cm^{-2}) the metal electrodes roughen[11] and at high temperatures oxides form, making the material less inert, and electrochemical interpretation more complicated.[19] Furthermore, the usable potential region becomes narrower when the temperature increases, which for electrocatalytic materials such as Pt is especially a problem.[20] Glassy carbon electrodes have also been employed in both laser heated[21] and Joule heated experiments[22] but were not robust enough for high temperature electrochemistry. In some cases the electrode was even found to combust.[22]

Boron doped diamond (BDD) has emerged as an important electrode material due to its unique properties such as wide potential window, chemical and mechanical robustness and low background currents.[23] These arise from the electrochemical stability of the surface brought about by the sp^3 bonding configuration of this non-metallic material. Furthermore, large area free-standing polycrystalline BDD (pBDD) can now be grown using microwave plasma chemical vapour deposition (MW-CVD) techniques[24] making applications more widespread. As the boron doping level in diamond is increased the resistivity decreases. The material becomes metal-like at B dopant concentrations > 1 × 10^{20} B atoms cm^{-3}.[23, 25] Crucially, BDD also possesses a very high thermal conductivity, ca. 600 W m^{-1} K^{-1} at 300 K,[26] for comparison the thermal conductivity of

copper is ca. 400 W m^{-1} K^{-1}.[27] The thermal diffusivity of metallic pBDD is approximately 2-3 times higher than that of a metal; hence the entire electrode should rapidly attain a relatively uniform temperature, even when heated from the rear. Being mechanically robust, pBDD electrodes can be made very thin, and hence have a very low thermal mass. Thus high electrode temperatures can be achieved with modest input powers. Diamond oxidises in air only if heated over ca. 700 °C.[28] Previous studies investigating laser damage to diamond have shown the laser damage threshold for intrinsic polished polycrystalline diamond to be typically in excess of 1.5 GW cm^{-2} for nanosecond (ns) pulses.[29]

In this discussion paper, given the notably favourable properties of conducting diamond, we examine the use of pBDD as an electrode material for thermoelectrochemical studies. In particular using pulsed laser heating methodology we examine the redox behaviour of two different fast electron transfer outer sphere redox species at a macrodisk pBDD electrode, in widely different potential ranges, under heated conditions.

2 Experimental

***Solutions*:** All solutions were prepared using Milli-Q water (resistivity 18.2 MΩ cm at 25 °C) and all reagents were used as received. The supporting electrolyte employed was 0.1 M potassium nitrate (KNO_3, Sigma-Aldrich, 99 %) unless otherwise stated. Redox solutions contained either 1 mM ruthenium (III) hexaamine chloride ($Ru(NH_3)_6^{3+}$, Acros Organics, 98%) or 1 mM potassium hexachloroiridate (III) ($IrCl_6^{3-}$, Sigma-Aldrich, 98%). For open circuit potential measurements, potassium ferricyanide (III) ($Fe(CN_6)^{3-}$, Sigma-Aldrich, 99%), potassium hexacyanoferrate (II) trihydrate ($Fe(CN_6)^{4-}$, Sigma-Aldrich, ≥98.5%), ruthenium (II) hexaamine chloride ($Ru(NH_3)_6^{2+}$, Acros Organics, > 99%) and potassium hexachloroiridate (IV) ($IrCl_6^{2-}$, Sigma Aldrich, 98%) solutions were also employed.

***Pulsed Laser Heating Set-up*:** A 9 mm diameter disk of freestanding conducting pBDD synthesised by MW-CVD (boron dopant level ~ 3×10^{20} B atoms cm^{-3}), was grown by Element Six (Harwell, Oxford). The pBDD was removed from the growth substrate and polished (lapped) on both sides to give a surface finish of 1.25 ± 0.05 nm (measured over typical areas of 20 μm × 20 μm). The resulting thickness of the electrode was 200 μm. The electrode was ohmically back contacted by sputtering (Edwards E606 sputterer) Ti (20 nm) / Au (400 nm) and annealing in a tube furnace for 5 hr at 450 °C. In order to perform electrochemical measurements during pulsed heating, a custom-built electrochemical cell was designed and fabricated in-house. The cell comprised two parts, a Teflon® container and a Perspex® window, held together with nylon screws. The Perspex® window contained a hole in the centre, across which the black pBDD disk was mounted (inside face) and held in place with adhesive Kapton® tape (100 μm thickness, stable up to 1000 °C, R.S. Components Ltd.). The electrode area exposed to solution was reduced, also using Kapton® tape, which contained a laser micromachined circular hole, 1 mm in diameter. A conductive track was made from the annealed Ti/Au contact on the back face of the pBDD electrode (which is not in contact with solution) using silver conductive paint (R.S. Components Ltd.) to the top of the Perspex® window, where electrical contact was made with a crocodile clip. The experimental set-up is shown in **Figure 1**.

For the majority of experiments, cyclic voltammetry (CV) was performed simultaneously with pulsed laser heating *i.e.* temperature pulse voltammetry (TPV). All electrochemical experiments utilised a three electrode setup controlled by a potentiostat;

(CompactStat, Ivium Technologies, The Netherlands) connected to a laptop computer. A thick coiled Pt wire was used as the counter electrode and a commercial saturated calomel electrode (SCE: CHI150, CH Instruments Inc. TX) served as the reference electrode. A diode laser (LM-D0296, LIMO) 914.7 nm, 30 W, was used for all pulsed temperature experiments, controlled by a laser diode controller (LDC1000, Laser Electronics Ltd Lincolnshire, England). The delivery lens focused the laser to a 1 mm diameter central circular spot on the back face of the BDD electrode. A dual-channel function generator (AFG3022B, Tektronix) was used as a master controller for TPV experiments to ensure that the potentiostat and laser were synchronised when manually triggered. For the majority of experiments the CV potential scan rate was fixed at 100 mV s^{-1} (0.25 mV step potential). P_d was varied between 0.3 kW cm^{-2} and 3.8 kW cm^{-2} in conjunction with a laser duty cycle (ratio of laser on to off time) of 10 ms on (smallest pulse width that could be effectively employed) and 90 ms off.

Open circuit potential (OCP) measurements: OCP measurements were carried out using an isothermal approach to determine the temperature coefficient, $\beta = (\delta OCP/\delta T)$, for the different redox couples employed. A heated water bath attached to a jacketed glass cell was used to control the temperature of the electrochemical system. For OCP measurements three separate solutions were employed containing either (1) 0.5 mM $Fe(CN)_6^{4-}$ and 0.5 mM $Fe(CN)_6^{3-}$; (2) 0.5 mM $Ru(NH_3)_6^{3+}$ and 0.5 mM $Ru(NH_3)_6^{2+}$ or (3) 0.5 mM $IrCl_6^{3-}$ and 0.5 mM $IrCl_6^{2-}$. In all cases, one of the solutions was held at an elevated temperature using the jacketed cell, in the range 23 °C - 63 °C, whilst the other was maintained at ambient temperature (23 °C). The two solutions were connected with a saturated KNO_3 salt bridge. Two conducting BDD, glass-sealed 1 mm diameter macrodisk electrodes, were constructed as described previously,[30] placed in the separate solutions and connected to a high impedance digital voltmeter. OCPs were recorded as a function of the temperature difference, ΔT, between the two solutions.

Atomic Force Microscopy (AFM): AFM measurements were recorded in Tapping Mode™ with an Enviroscope equipped with Nanoscope IV controller (Bruker, UK).

COMSOL simulations: A model for simulating the induced temperature profile upon application of the laser pulse as well as the effect of the fluctuating temperature on convection, diffusion and thermodynamics was carried out using COMSOL Multiphysics 4.3b (COMSOL, Sweden) finite element modelling (FEM) software. A *2D* geometry, shown in **Figure 2** (not to scale) was built to describe the *2D* axisymmetric electrochemical cell. The model consists of the pBDD electrode, thickness 200 µm and 4.5 mm radius (domain a), mounted in Perspex®, (domain d), insulated with Kapton® tape, thickness 100 µm, (domain b), which also defines the radius of the electrode (0.5 mm) in contact with solution (domain c). The radius and height of the modelled system is 12.5 mm. Each domain is occupied by material with a defined density (ρ), heat capacity (C_p), thermal conductivity (κ) and dynamic viscosity (μ), as detailed in **Table 1**. The pressure constraint point (P_{con}), which is necessary for the solved equations to have a unique solution, in **Figure 2** was set to 1 atm. The location selected for this constraint was such that the solution was not significantly perturbed. The boundary conditions are summarised in **Table 2**. In **Table 2**, P (W) and A (cm^2) represent the total boundary power and the active area and $\boldsymbol{n}$ is the unit normal vector. A no heat flux boundary condition is applied to boundary 2 (thermal insulator). No slip conditions were applied for boundaries 5 and 6. Gravity has an effect on the flow pattern of the fluid and thus a volume force (f_z) acting only in the z-dimension defined as

$$f_z = -\rho g \quad (1)$$

where g is the gravitational constant (~9.81 m s^{-2}), was employed.

Heat transfer involves various mechanisms, such as thermal diffusion, thermal convection, thermal radiation, *etc*. These mechanisms often occur simultaneously in the system. Thermal diffusion of heat from a region of high temperature to low temperature is described by **Equation 2**, for both solids and liquids, where α_D, the thermal diffusivity (m^2 s^{-1}) is given by **Equation 3**,

$$\frac{\partial T}{\partial t} = \alpha_D \nabla^2 T \quad (2)$$

$$\alpha_D = \frac{\kappa}{\rho C_p} \quad (3)$$

where t (s) represents time, and ∇^2 is the Laplace operator.

Convective flow of water in the system is treated as an incompressible flow of a Newtonian fluid which follows the Navier-Stokes equation, **Equation 4**,

$$\rho\left(\frac{\partial \boldsymbol{v}}{\partial t} + \boldsymbol{v} \cdot \nabla \boldsymbol{v}\right) = -\nabla p + \mu \nabla^2 \boldsymbol{v} + f_z \quad (4)$$

where $\boldsymbol{v}$ (m s^{-1}) is the flow velocity, p (pa) is the pressure and ∇ is the grad operator.

A boundary heat source (boundary 1), reflecting P_d values in the range 0.3 kW cm^{-2} to 3.8 kW cm^{-2}, was employed to model the laser spot on the back of the diamond electrode. At t = 0 s, a laser pulse of 10 ms is applied to the centre of the electrode (1 mm in diameter), followed by 90 ms cooling time. The modelled temperature at the electrode-electrolyte interface is the average temperature across the 1 mm diameter electrode surface.

Simulation of the effect of laser heating on TPV was performed by considering the effect of the temperature pulses and corresponding transient perturbations in T on the mass transport properties, kinetics and thermodynamics of the system, as described by **Equations 5 – 11**. Transport of dilute species in solution depends on convection, migration and diffusion. Migration was ignored due to the presence of excess supporting electrolyte (0.1 M KNO_3). In the fluid phase, the contribution of diffusion and convection is given by:

$$D_i \nabla C_i + \boldsymbol{v} \nabla C_i = 0 \quad (5)$$

where D_i and C_i are the diffusion coefficient and concentration of the species respectively. The effect of changing T on D_i was calculated using the Stokes-Einstein equation: [31]

$$D_i = \frac{k_B T}{6\pi\mu r} \quad (6)$$

where k_B is the Boltzmann constant and r is the radius of the molecule. r for $Ru(NH_3)_6^{3+}$ was determined as 0.28 nm using **Equation 6** , and a literature value[32] for D at 298 K of 8.8×10^{-6} cm^2 s^{-1} and is assumed to be temperature independent. The T induced change in μ is accounted for in the water material characteristics, as described in **Table 1**.

Simple outer sphere electron transfer was modelled at the electrode-solution interface (boundary 5) using Butler-Volmer (BV) kinetics. The current at the electrode, i_{elec}, is determined by:

$$i_{elec} = nAFj_{elec} \quad (7)$$

where n is the number of electrons transferred per redox species, A is the area of the electrode, F is Faraday's constant and j_{elec} is the flux of species at the electrode surface, defined by:

$$j_{elec} = k_f C_{ox,elec} - k_b C_{red,elec} \quad (8)$$

where k_f and k_b are the reaction rates of the forward and back reactions respectively, described by:

$$k_f = k^0 e^{\frac{\alpha n F\left(E-(E^0+\beta\Delta T)\right)}{RT}} \quad (9)$$

$$k_b = k^0 e^{\frac{(1-\alpha) n F\left(E-(E^0+\beta\Delta T)\right)}{RT}} \quad (10)$$

where α is the charge transfer coefficient, here assumed to be 0.5, E is the electrode potential, E^0 is the standard potential (-0.18 V vs. SCE), R is the gas constant and ΔT is the change in temperature at the electrode/electrolyte interface. The standard rate constant (k^0) is temperature dependent, described by the Arrhenius equation,

$$k^0 = A\, e^{\frac{-E_a}{RT}} \quad (11)$$

where E_a is the activation energy, A is the pre-exponential factor, which is considered to be temperature independent. For $Ru(NH_3)_6^{3+/2+}$ A is calculated as 1026 cm s^{-1} assuming a literature value of 22.5 kJ mol^{-1} [33] for E_a and k^0 = 0.1 cm s^{-1} [34] at 293.15 K (**Equation 11**).

3 Results and Discussion

For all TPV experiments the basic premise is imposition of a pulsed laser to heat the surface of the electrode during CV. In CV, for a chosen scan rate and potential step, the number of data points are defined by scan rate/potential step and the time between potential steps is given by (number of data points)$^{-1}$. For the CV experiments described herein (using commercial software) the current is sampled immediately after each potential step. In TPV, the temperature pulse is superimposed on top of the CV and the current recorded, as shown schematically in **Figure 3**. For the majority of experiments the laser is switched on and the electrode heated for the shortest time possible, 10 ms, and then switched off for 90 ms, with the cycle continuously repeated. For typical experimental parameters of 100 mV s^{-1} and 0.25 mV potential step, current values are collected every 2.5 ms, with a total of 400 data points per second.

Verification of the time-dependant average temperature at the front face of the BDD electrode during the laser pulse experiments was made from both measurement of the OCP (**Figure 4a**) and thermal modelling (**Figure 4b**), described in **Section 2**. β was calculated as -1.56 mV K^{-1} for $Fe(CN)_6^{3-}/Fe(CN)_6^{4-}$, from a plot of OCP versus ΔT (R^2 = 0.98) over the ΔT range of 40 °C. This value is in very good agreement with that determined previously, -1.6 mV K^{-1}.[35] With knowledge of β and the measured OCP, during laser heating, the corresponding interfacial electrode ΔT, versus time, t, behaviour can be determined; **Figure 4a** shows the OCP and ΔT data for a P_d of 0.6 kW cm^{-2}, 1.2 kW cm^{-2} and 3.2 kW cm^{-2} over a period of 90 ms (the laser is on for the first 10 ms). The data shows that during the laser pulse period, the temperature rises rapidly at the electrode surface. After the laser is turned off, the temperature decreases at a slower rate due to the lower value of thermal diffusivity for water, hindering heat transfer to bulk solution. For different P_d values in the range 0.3 kW cm^{-2} to 3.8 kW cm^{-2}, maximum T values at t_{10ms} at the electrode/electrolyte interface in the range 31.0 to 90.0 °C were obtained. Specifically, 31.0 °C (0.3 kW cm^{-2}); 36.5 °C (0.6 kW cm^{-2}); 41.5 °C (0.9 kW cm^{-2}); 46.4 °C (1.2 kW cm^{-2}); 51.6 °C (1.6 kW cm^{-2}); 57.3 °C (1.9 kW cm^{-2}); 62.9 °C (2.2 kW cm^{-2}); 68.4 °C (2.5 kW cm^{-2}); 73.1 °C (2.9 kW cm^{-2}); 78.9 °C (3.2 kW cm^{-2}); 84.1 °C

(3.5 kW cm^{-2}) and 90.0 ^{o}C (3.8 kW cm^{-2}). **Figure 4b** shows the ΔT profile determined from FEM simulations for a P_d of 0.6 kW cm^{-2}, 1.2 kW cm^{-2} and 3.2 kW cm^{-2} over 90 ms (the laser is on for the first 10 ms). Also given in the inset is a comparison of the recorded ΔT for the two methodologies; OCP (■) and FEM modelling (•). As can be seen there is very good agreement between both methods of temperature determination. The employment of a higher P_d would allow even greater ΔT values to be reached.

To visualise propagation of the thermal gradient through the pBDD electrode and into solution during the laser pulse as a function of time, thermal modelling was performed. **Figure 5a** shows the 2D temperature profile at t = 10 ms (*i.e.* at the end of the laser pulse) and **Figure 5b** the z axial temperature profile (about the central axis of symmetry, r = 0) as a function of time, t = 0, 5, 10 and 20 ms for a P_d of (i) 1.2 kW cm^{-2} and (ii) 3.2 kW cm^{-2}, respectively. As Figure 5a shows, for both P_d values, heat diffuses out from the laser heated zone hemispherically, diffusing much faster through the 200 μm thick pBDD than the surrounding solution, due to the higher thermal diffusivity of the conducting diamond. At both t = 5 ms and t = 10 ms (the end of the laser pulse), there is a small gradient in temperature through the BDD electrode which increases in absolute value as both P_d and t increases. The thermal gradient extends ca. 200 μm (1.2 kW cm^{-2}) and 230 μm (3.2 kW cm^{-2}) from the electrode surface into solution. At t = 20 ms, after the laser has been switched off for 10 ms, ΔT has decreased significantly in the electrode (with a uniform T obtained vertically through the pBDD). The water, however, as it retains heat more effectively, due to a higher C_p, has a higher T than that of the diamond (at a defined distance from the electrode) as the pBDD is able to cool itself more rapidly.

With optical heating it is sensible to consider the laser damage threshold of the electrode material employed, especially as metallic pBDD absorbs very strongly at the wavelength (914 nm) of the diode laser employed herein. Previous studies indicate a laser damage threshold for intrinsic polycrystalline diamond typically to be in excess of 1.5 GW cm^{-2} for ns pulses,[29] which is far higher than the conditions employed here. This is verified in **Figure 6** which shows typical AFM images recorded in tapping mode at a scan rate of 20 μm s^{-1} before (a) and after (b) applying a P_d of 1.2 kW cm^{-2} (10 ms on, 90 ms off) for 120 cycles, typical to conditions employed herein. It can be seen from **Figure 6a** that the typical surface roughness of the pBDD electrode is 1.25 ± 0.05 nm before laser heating, compared to 1.3 ± 0.1 nm after. The AFM images in Figure 6 thus indicate no change in surface morphology at these modest fluxes. Note, this is in stark contrast to Pt electrodes which showed surface roughening with the electrode exposed to a P_d three orders of magnitude lower, for a similar timescale of exposure, but with ns laser pulses.[11] We are thus confident that much shorter and higher P_d pulses could be used in conjunction with BDD electrodes in order to establish significantly higher temperatures at the pBDD electrode/electrolyte interface.

Initial experiments investigated the effect of pulsed temperature on the non-faradaic response of the electrode as a function of P_d (0, 0.6 kW cm^{-2}, 1.2 kW cm^{-2} and 3.2 kW cm^{-2}). **Figure 7** shows the current-time response in 0.1 M KNO_3 with the electrode held at a constant potential of 0 V vs. SCE for a P_d of 0.6 kW cm^{-2}, 1.2 kW cm^{-2} and 3.2 kW cm^{-2}, with an increased data sampling frequency of 1 kHz. The laser was pulsed on for 10 ms and off for 90 ms. Also shown is the current-time response (black line) under ambient conditions. It can be seen in **Figure 7** that higher P_d and hence larger temperature changes produce bigger current transients. The inset shows a zoomed out current-time trace recorded over 1 s. Each trace has a peak, which is associated with the laser pulse turning on and a reverse peak associated with the laser pulse turning off. The largest change in both cases

occurs during the first ms and then the current transient decays.

Previous studies of the double layer using ns laser pulse techniques have shown that thermal heating leads to a virtually instantaneous restructuring of the double layer. The time constant of the data capture system employed herein is insufficient to probe such fast events, but still shows an effect. In particular, the current rise is associated with perturbation of the double layer resulting in a charging current, which decays with time in a similar fashion to a potential step experiment carried out under isothermal conditions. When the laser is turned off the temperature at the interface decreases to its original value, and due to restoration of the double layer, a current transient in the opposite direction is observed. The charge associated with the positive and negative current transients is approximately equal. For a P_d of 0.6 kW cm^{-2}, 1.2 kW cm^{-2} and 3.2 kW cm^{-2} , the charge transferred for both positive and negative transients is 0.31 nC and 0.30 nC, 0.49 nC and 0.48 nC, 0.95 nC and 0.91 nC, respectively.

Experiments investigating the effect of TPV on faradic processes were conducted by using a fast (reversible) one electron transfer outer sphere redox mediator, 1 mM $Ru(NH_3)_6^{3+}$ in 0.1 M KNO_3. The experimental TPV data is shown in **Figure 8a** and **Figure 8b** for the forward scan and backward scan respectively, under temperature pulsed (P_d of 1.2 kW cm^{-2}, pulse on 10 ms, off 90 ms) conditions (red line). The ambient CV (black line) for $Ru(NH_3)_6^{3+}$ reduction and subsequent oxidation shows a peak-to-peak separation of 65 mV and a reductive peak current of 2.18 μA in accordance with that predicted using the Randles-Sevick equation, assuming an electrode diameter of 1 mm and diffusion coefficient of 8.8 × 10^{-6} cm^2 s^{-1}.[32]

During TPV current spikes are obtained during laser heating, which decay during cooling, in a similar way to chronoamperometric transients produced during potential pulsing. A scan rate of 100 mV s^{-1} with a potential step of 0.25 mV is employed (sampling rate = 400 s^{-1}), resulting in 4 data points per laser pulse, where the last point records the largest current reading. Raw data is collected by the potentiostat (**Figures 8a** and **8b,** red line) and then sampled by taking every 40th point, resulting in the last sampling point during the laser pulse being plotted against potential. **Figure 8c** shows "data sampled" TPV responses at P_d of 1.2 kW cm^{-2} (red line) and 2.5 kW cm^{-2} (green line).

Three striking features are observed in the "data sampled" laser pulsed TPV, compared to the CV recorded under ambient condition; (1) the cathodic current for the forward scan increases as P_d increases. Specifically, the peak current has increased compared to that under ambient conditions by × 3.5 for 1.2 kW cm^{-2} and × 8.1 for 2.5 kW cm^{-2}. (2) The potential for the forward peak current shifts positively with increasing P_d (-0.168 V for 1.2 kW cm^{-2} and -0.148 V for 2.5 kW cm^{-2}) and; (3) a cathodic current is observed in magnitude for the backward scan, which increases in magnitude as the P_d is increased. β for the $Ru(NH_3)_6^{3+/2+}$ system, was calculated as +0.68 mV K^{-1} from a plot of OCP versus ΔT (R^2 = 0.99) over a ΔT range of 40 ^{o}C, in close agreement with literature values.[11] From knowledge of β it is possible to calculate the change in entropy of the system, ΔS, through

$$\Delta S = nF\beta = 65.6 \text{ J K}^{-1}\text{mol}^{-1} \quad (12)$$

given n = 1.

The increase in cathodic (negative) current in the forward scan and

observation of a cathodic current in the backward scan is due primarily to a combination of two factors, the entropy of the redox reaction and a change in mass transport due to the induced thermal gradient at the electrode/electrolyte interface. In these experiments, the temperature at the electrode/electrolyte interface is pulsed from ambient to hot repeatedly. Entropically, under steady-state conditions, a positive β indicates an additional cathodic current contribution to the ambient response (for both redox processes), near to the equilibrium potential.[36] Furthermore, the transient nature of the temperature increase also results in time-dependant increases in mass transport, due to both diffusion and convective effects, which serves to enhance the current relative to ambient conditions. By modelling all the contributions described in **Section 2**, qualitatively similar TPVs can be obtained, as shown in the inserts to **Figures 8a** and **8b**. The small discrepancy between model and experiment is likely to be due to employment of a 2D axisymmetric model. This model does not account for the fact the laser strikes the electrode perpendicular to the direction of gravity, instead a computationally less time consuming parallel arrangement was assumed, which is likely to underestimate convective water flow effects. More sophisticated 3D simulations are currently in progress.

In order to further explore the effect of TPV on redox electrochemistry, another fast electron transfer (reversible) outer sphere redox mediator, $IrCl_6^{3-}$, was employed. Isothermal experiments gave a β value of -0.48 mV K^{-1} (R^2 = 0.99) for $IrCl_6^{3-/2-}$ (ΔS = -46.3 J K^{-1} mol^{-1}) recorded over a ΔT range of 40 ^oC. **Figure 9** shows a "data sampled" TPV (data collected as described for **Figure 8c**) for a pBDD electrode in a solution containing 1 mM $IrCl_6^{3-}$ in 0.1 M KNO_3, at a scan rate of 100 mV s^{-1} for P_d of 0.6 kW cm^{-2}, 1.2 kW cm^{-2}, 1.9 kW cm^{-2} and 2.5 kW cm^{-2}. Under ambient conditions the CV for $IrCl_6^{3-}$ oxidation and subsequent reduction shows a peak-to-peak separation of 70 mV and an oxidative peak current of 1.96 µA in agreement with Randles-Sevick predictions, assuming an electrode diameter of 1 mm and diffusion coefficient of 7.5×10^{-6} cm^2 s^{-1}.[37] It can be seen in **Figure 9** that (i) the anodic peak current for the forward scan increases as P_d increases; (ii) the potential for the forward peak current shifts negatively with increasing P_d, as expected for a negative β value (0.731 V for 0.6 kW cm^{-2}; 0.711 V for 1.2 kW cm^{-2}; 0.691 V for 1.9 kW cm^{-2}; and 0.681 V for 2.5 kW cm^{-2}) and; (iii) as P_d increases the "data sampled" back scan TPV shows a very small cathodic current at 0.6 kW cm^{-2}, which disappears at higher P_d, resulting in the observation of double peaked anodic currents at the two highest P_d values. The data shown is thus in qualitative agreement with that seen for the $Ru(NH_3)_6^{3+}$ TPV system (**Figure 8**).

4 Conclusions

An electrochemical system combined with a pulsed laser setup is employed to examine the effect of temperature on the electrochemical response of pBDD electrodes. Conducting diamond is an ideal material for thermoelectrochemical studies due to its wide potential window, low background currents, very high thermal conductivity and thermal diffusivity, mechanical robustness and ability to withstand P_d up to GW cm^{-2} without damage, for ns pulses. In these measurements, laser pulses of 10 ms duration (90 ms off) were delivered using a focused diode laser (maximum P_d 3.8 kW cm^{-2}) onto a ~ 1 mm spot on the rear side of a 200 µm thick pBDD electrode. The temperature attained at the pBDD electrode/electrolyte interface during this time period was assessed using both OCP measurements and

FEM simulations; with both methods providing good agreement. A maximum temperature of 90.0 ^{o}C was achieved at the electrode/electrolyte interface using a P_d of 3.8 kW cm^{-2} for a heating time of 10 ms. Due to the high thermal diffusivity of pBDD, heat propagates into the electrode rapidly, without damage to the electrode surface, as evidenced by AFM. As diamond can withstand significantly greatly power densities even higher temperatures can be attained quickly by moving to significantly higher power lasers.

TPV measurements in supporting electrolyte were found to perturb the double layer, resulting in a positively peak-shaped charging current when the laser was on and restoration of the double layer, accompanied with a negative charging current, when the laser was turned off. The total charge transferred during the switch on and off periods was found to be approximately equal. In the presence of the fast electron transfer (reversible) outer sphere redox mediators, $Ru(NH_3)_6^{3+}$ (β = +0.68 mV K^{-1}) and $IrCl_6^{3-}$ (β = -0.48 mV K^{-1}), TPV resulted in chronoamperometric-like current increases during the CV which enhanced the forward peak current, increasing with increasing P_d. The peak potentials were shifted positively for $Ru(NH_3)_6^{3+/2+}$ and negatively for $IrCl_6^{3-/2-}$, compared to the CV recorded under ambient conditions, in accordance with their entropic positive and negative β values, respectively. Scanning backwards cathodic ($Ru(NH_3)_6^{3+/2+}$) and anodic ($IrCl_6^{3-/2-}$) peaked current response were also observed (leading to the observation of a double peak). FEM showed striking qualitative agreement with the experimental data obtained and differences are most likely due to constraints imposed due to technical limitations of the approach used. pBDD is thus a promising electrode material for high temperature thermoelectrochemical measurements. We plan to extend these studies by using higher power lasers to further increase the surface temperature and examine the effect of temperature on industrially relevant electrochemical processes.

Acknowledgements

JI acknowledges support from the EPSRC Analytical Fund. LM and MJ would like to thank the University of Warwick Chancellors International Scholarship Scheme and Element Six respectively for financial support. We acknowledge Prof. Patrick Unwin for helpful discussions. We all thank Mr. Jon Newland (Warwick Chemistry) for photographing the experimental setup and Element Six for providing the pBDD used in these studies.

References

[a] *Department of Chemistry, University of Warwick, Coventry, UK. Fax: 02476524112; Tel: 02476 573886; E-mail: j.macpherson@warwick.ac.uk*
[b] *Department of Physics, University of Warwick, Coventry, UK.: Fax:02476150897; Tel:02476 150799; E-mail: m.e.newton@warwick.ac.uk*

1. C. G. Ubah and E. Asselin, *ECS Trans.*, 2009, 19, 3-20.
2. J. Zhang, Z. Xie, J. Zhang, Y. Tang, C. Song, T. Navessin, Z. Shi, D. Song, H. Wang and D. P. Wilkinson, *J. Power Sources*, 2006, 160, 872-891.
3. P. Gründler, A. Kirbs and L. Dunsch, *ChemPhysChem*, 2009, 10, 1722-1746.
4. C. L. Forryan and R. G. Compton, *Phys. Chem. Chem. Phys.*, 2003, 5, 4226-4230.
5. S. H. Joo, S. J. Choi, I. Oh, J. Kwak, Z. Liu, O. Terasaki and R. Ryoo, *Nature*, 2001, 412, 169-172.
6. K. Gong, F. Du, Z. Xia, M. Durstock and L. Dai, *Science*, 2009, 323, 760-764.
7. P. V. Rysselberghe, *Electrochemical Affinity: Studies in Electrochemical Thermodynamics and Kinetics*, Paris, 1955.

8. G. G. Wildgoose, D. Giovanelli, N. S. Lawrence and R. G. Compton, *Electroanalysis*, 2004, 16, 421-433.
9. G. Barker and A. Gardner, *J. Electroanal. Chem. Interfacial Electrochem.*, 1975, 65, 95-100.
10. E. Hershenhart, R. L. McCreery and R. D. Knight, *Anal. Chem.*, 1984, 56, 2256-2257.
11. R. P. Akkermans, M. F. Suárez, S. L. Roberts, Q. Fulian and R. G. Compton, *Electroanalysis*, 1999, 11, 1191-1202.
12. J. L. Brennan and R. J. Forster, *J. Phys. Chem. B*, 2003, 107, 9344-9350.
13. J. F. Smalley, C. Krishnan, M. Goldman, S. W. Feldberg and I. Ruzic, *J. Electroanal. Chem. Interfacial Electrochem.*, 1988, 248, 255-282.
14. J. F. Smalley, S. W. Feldberg, C. E. Chidsey, M. R. Linford, M. D. Newton and Y. P. Liu, *J. Phys. Chem.*, 1995, 99, 13141-13149.
15. A. Yamakata, T. Uchida, J. Kubota and M. Osawa, *J. Phys. Chem. B*, 2006, 110, 6423-6427.
16. T. Hinoue, R. Harui, T. Izumi, I. Watanabe and H. Watarai, *Anal. Sci.*, 1995, 11, 1-8.
17. V. Climent, B. A. Coles and R. G. Compton, *J. Phys. Chem. B*, 2002, 106, 5988-5996.
18. T. Hinoue, N. Kuwamoto and I. Watanabe, *J. Electroanal. Chem.*, 1999, 466, 31-37.
19. M. R. Mahoney and R. P. Cooney, *J. Phys. Chem.*, 1983, 87, 4589-4591.
20. P. Gründler, A. Kirbs and T. Zerihun, *Analyst*, 1996, 121, 1805-1810.
21. F. Qiu, R. G. Compton, F. Marken, S. J. Wilkins, C. H. Goeting and J. S. Foord, *Anal. Chem.*, 2000, 72, 2362-2370.
22. P. Gründler, T. Zerihun, A. Möller and A. Kirbs, *J. Electroanal. Chem.*, 1993, 360, 309-314.
23. L. A. Hutton, J. G. Iacobini, E. Bitziou, R. B. Channon, M. E. Newton and J. V. Macpherson, *Anal. Chem.*, 2013, 85, 7230-7240.
24. R. Balmer, J. Brandon, S. Clewes, H. Dhillon, J. Dodson, I. Friel, P. Inglis, T. Madgwick, M. Markham and T. Mollart, *J. Phys.: Condens. Matter*, 2009, 21, 3-5.
25. J. P. Lagrange, A. Deneuville and E. Gheeraert, *Diamond Relat. Mater.*, 1998, 7, 1390-1393.
26. J. E. Field, *The properties of natural and synthetic diamond*, Academic Press London, 1992.
27. K. Yoshida and H. Morigami, *Microelectron. Reliab.*, 2004, 44, 303-308.
28. P. John, N. Polwart, C. Troupe and J. Wilson, *Diamond Relat. Mater.*, 2002, 11, 861-866.
29. R. Sussmann, G. Scarsbrook, C. Wort and R. Wood, *Diamond Relat. Mater.*, 1994, 3, 1173-1177.
30. L. Hutton, M. E. Newton, P. R. Unwin and J. V. Macpherson, *Anal. Chem.*, 2008, 81, 1023-1032.
31. E. L. Cussler, *Diffusion: mass transfer in fluid systems*, Cambridge, 2009.
32. J. V. Macpherson, D. O'Hare, P. R. Unwin and C. P. Winlove, *Biophys. J.*, 1997, 73, 2771-2781.
33. F. Qiu, R. G. Compton, B. A. Coles and F. Marken, *J. Electroanal. Chem.*, 2000, 492, 150-155.
34. H. V. Patten, K. E. Meadows, L. A. Hutton, J. G. Iacobini, D. Battistel, K. McKelvey, A. W. Colburn, M. E. Newton, J. V. Macpherson and P. R. Unwin, *Angew. Chem. Int. Ed.*, 2012, 51, 7002-7006.
35. A. Olivier, E. Merienne, J. Chopart and O. Aaboubi, *Electrochim. Acta*, 1992, 37, 1945-1950.
36. J. Valdes and B. Miller, *J. Phys. Chem.*, 1989, 93, 7275-7280.
37. J. V. Macpherson, C. E. Jones and P. R. Unwin, *J. Phys. Chem. B*, 1998, 102, 9891-9897.

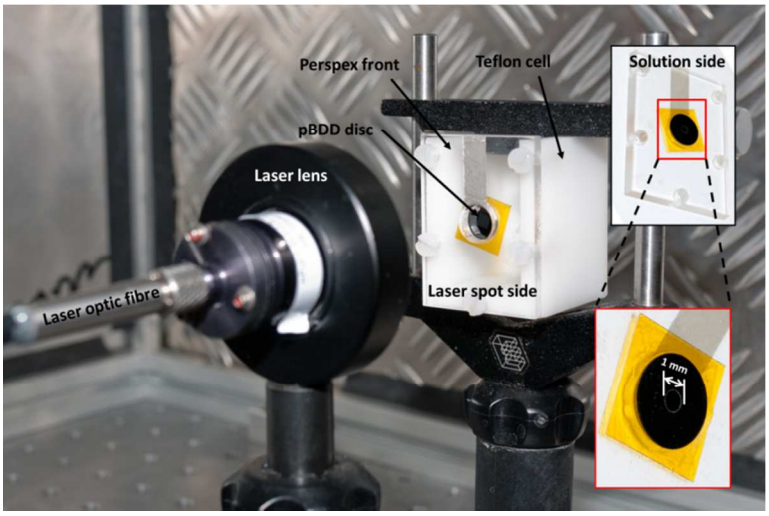

Figure 1: Photograph of the pulsed laser heating experimental set-up. The laser beam is focused by the laser lens onto the rear of the pBDD electrode held in the Perspex® cell. Insets show the solution facing side of the electrochemical cell, detailing the black pBDD held in place with Kapton® tape which also defines the active electrode area (1 mm disc).

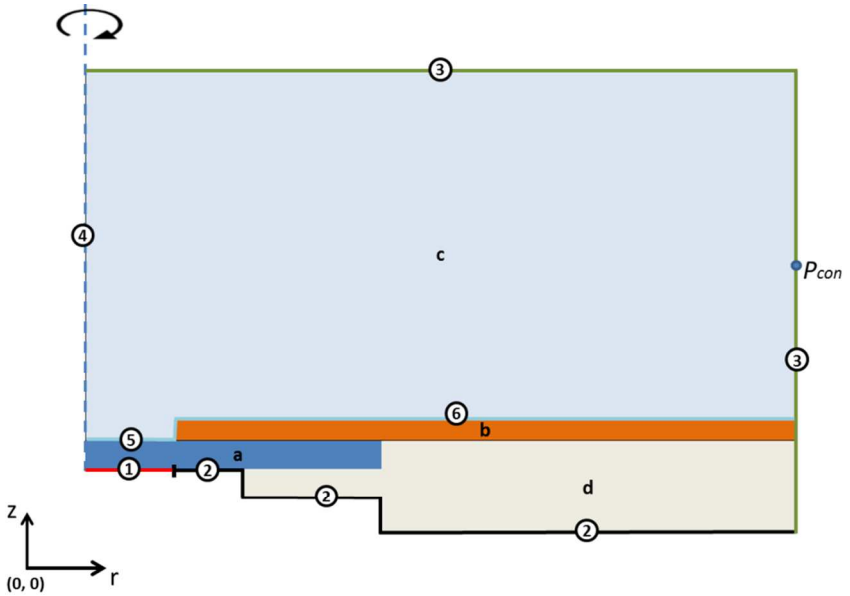

***Figure 2*:** Schematic of the simulated geometry (not to scale) of the electrochemical cell consisting of pBDD (a), Kapton® (b), water (c) and Perspex® (d).

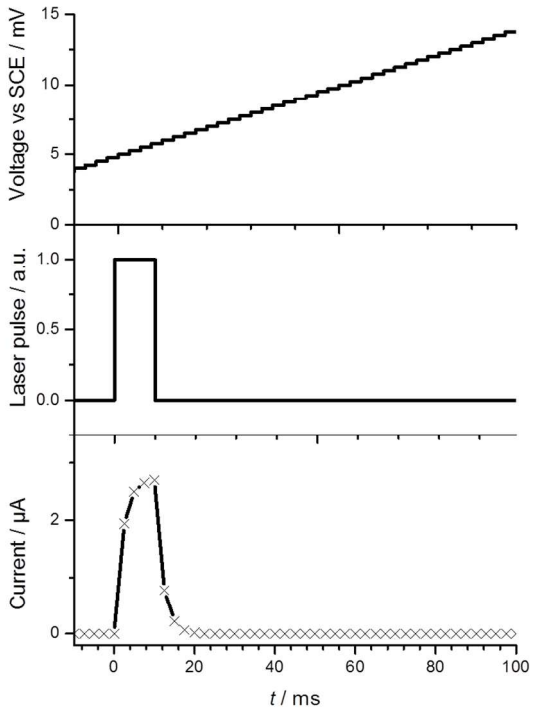

Figure 3: Schematic graphs showing the time dependance of (a) voltage steps taken by the digital potentiostat, (b) applied laser pulses (10 ms on and 90 ms off) and (c) change in current measured as a result of laser heating.

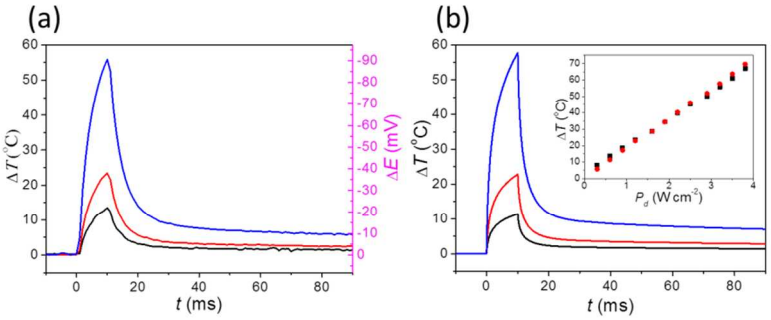

***Figure 4**:* (a) OCP and associated temperature rise (ΔT) versus time for a 90 ms time period, recorded between a laser heated 1 mm diameter pBDD disc electrode and a 1 mm diameter pBDD disc electrode at ambient temperature (23 °C). Solution contained 0.5 mM $Fe(CN)_6^{4-}$ and 0.5 mM $Fe(CN)_6^{3-}$ in 0.1 M KNO_3. The laser was pulsed at 0.6 kW cm^{-2} (black), 1.9 kW cm^{-2} (red) and 3.2 kW cm^{-2} (blue) for a 10 ms period and then switched off. The OCP data is converted to ΔT using the $Fe(CN)_6^{4-}$ / $Fe(CN)_6^{3-}$ temperature coefficient = -1.62 mV K^{-1}. (b) Finite element modelled ΔT (at the electrode surface) of the laser heated pBDD electrode at P_d = 0.6 kW cm^{-2} (black), 1.9 kW cm^{-2} (red) and 3.2 kW cm^{-2} (blue). Insert shows maximum ΔT as a function of P_d for both experimental (black ■) and simulation (red ●).

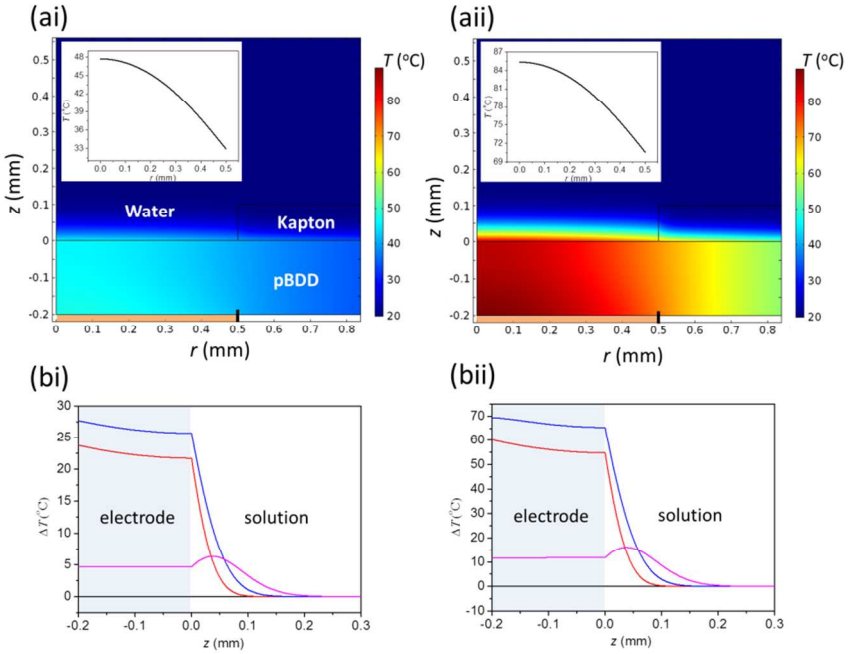

***Figure 5**:* (a) 2D temperature profile at t = 10 ms and (b) z axial temperature profile through pBDD to solution at r = 0 mm for times of 0 ms (black), 5 ms (red), 10 ms (blue) and 20 ms (purple) at P_d of 1.2 kW cm^{-2} (i) and 3.2 kW cm^{-2} (ii). The insets to (a) show radial temperature profiles at z = 0 mm (electrode surface) at t = 10 ms. The laser heated boundary in (a) is marked by an orange band and occurs at z = -0.2 and 0 < r < 0.5.

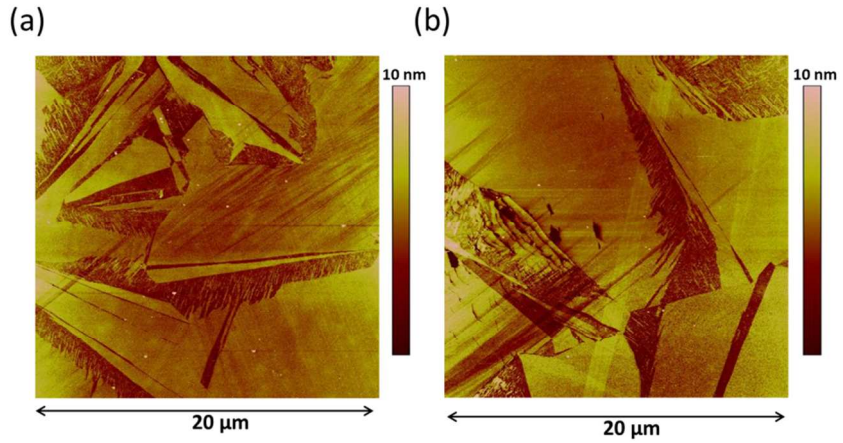

Figure 6: Typical tapping mode AFM images recorded at a scan rate of 20 µm s^{-1} before (a) and after (b) applying P_d of 1.2 kW cm^{-2} (10 ms on, 90 ms off) for 120 cycles.

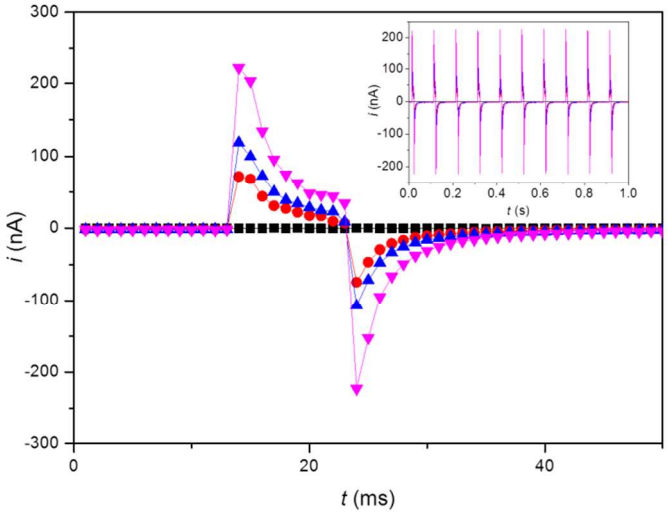

Figure 7: Temperature pulsed chronoamperometry of pBDD in 0.1 M KNO_3 at P_d of 0 W cm^{-2} (black ■), 0.6 kW cm^{-2} (red ●), 1.2 kW cm^{-2} (blue ▲) and 3.2 kW cm^{-2} (purple ▼) at an applied potential of 0 V *vs* SCE. Insert shows time-dependent current at the potential of 0 V vs. SCE for a duration of 1 s.

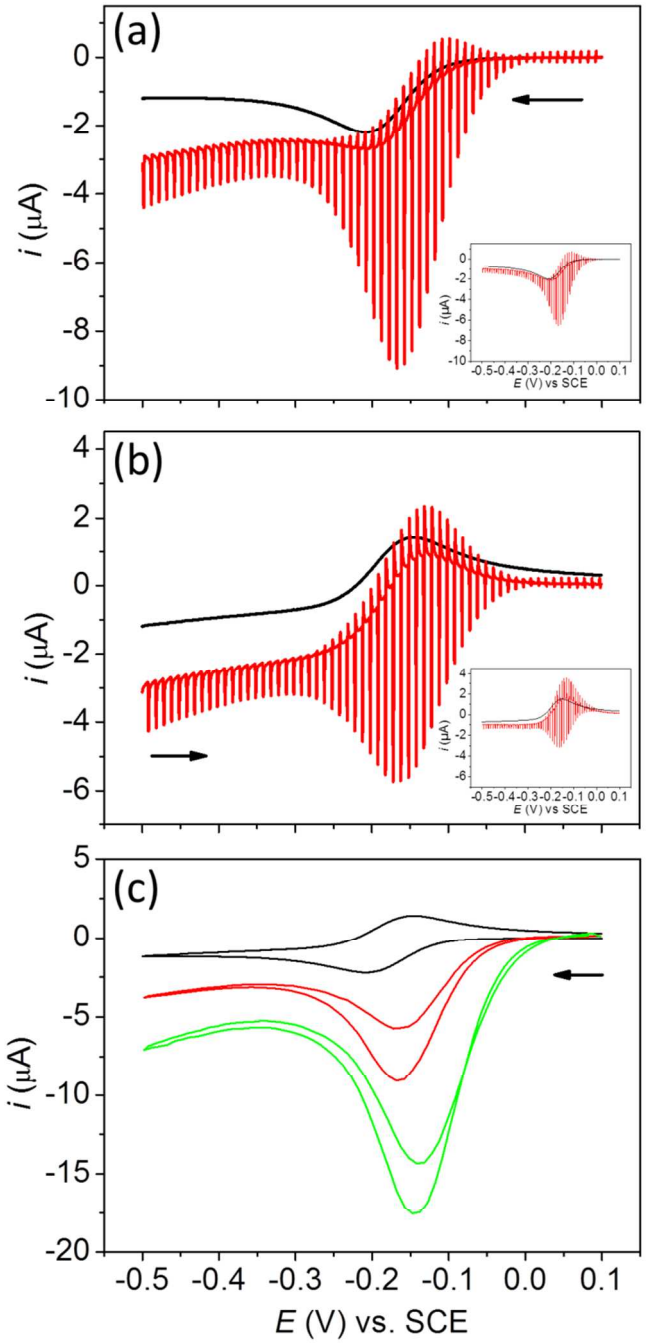

Figure 8: TPV (red) at P_d of 1.2 kW cm^{-2} and ambient CV (black) recorded at a pBDD electrode in a solution containing 1 mM $Ru(NH_3)_6^{3+}$ in 0.1 M KNO_3 (a) forward scan and (b) backward scan. Inserts in (a) and (b) show both the simulated TPV (red) at P_d of 1.2 kW cm^{-2} and ambient CV. (c) "Data sampled" experimental TPVs at a P_d of 1.2 kW cm^{-2} (red), and 2.5 kW cm^{-2} (green), every 40th data point sampled. The CV recorded under ambient conditions (black) is not data sampled. Scan rate: 100 mV s^{-1}.

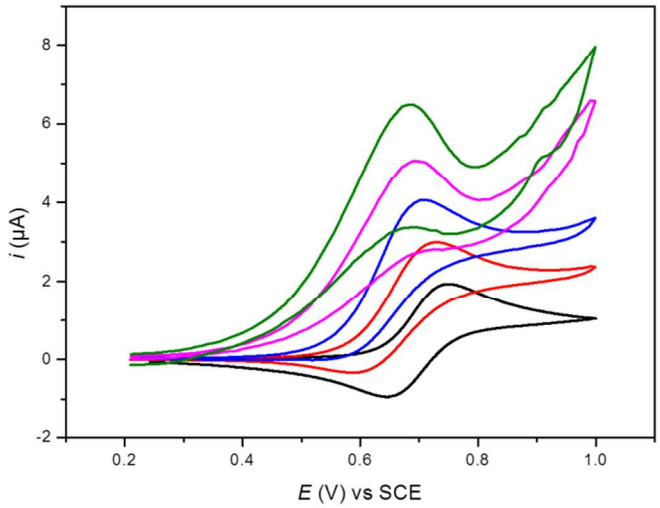

Figure 9: "Data sampled" TPV using a pBDD electrode in a solution containing 1 mM $IrCl_6^{3-}$ in 0.1 M KNO_3, at P_d of 0.6 kW cm^{-2} (red), 1.2 kW cm^{-2} (blue) , 1.9 kW cm^{-2}(purple) and 2.5 kW cm^{-2} (green). Every 40th data point is sampled. The CV recorded under ambient conditions (black) is not data sampled or subject to a laser pulse. Scan rate: 100 mV s^{-1}.

Table 1: Summary of the properties for the different domains used for the simulation of temperature at the diamond electrode/electrolyte interface

	Diamond [1]	**Kapton®** [2]	**Perspex®** [3]	**Water** [4]
Heat Capacity C_p (J kg^{-1} K^{-1})	$C_p = 3.2T - 473.6$ (275 K<T<500 K)	1090	1500	12010-80.4×T+0.310×T^2-5.38×10^{-4}×T^3+3.63×10^{-7}×T^4 (273.15 K<T<553.75K)
Density ρ (kg m^{-3})	3500	1420	1160	838+1.40×T-3.01×10^{-3}×T^2+3.72×10^{-7}×T^3 (273.15 K<T<553.75K)
Thermal Conductivity κ (W m^{-1} K^{-1})	-1.25T+1041.25 (275 K<T<500 K)	0.12	50	-0.869+8.95×10^{-3}×T-1.58×10^{-5}×T^2+7.98×10^{-9}×T^3 (273.15 K<T<553.75K)
Dynamic Viscosity μ (Pa·s)	N/A	N/A	N/A	1.38-2.12×10^{-3}×T+1.36×10^{-4}×T^2-4.65×10^{-7}×T^3+8.90×10^{-10}×T^4+9.08×10^{-13}×T^5+3.85×10^{-16}×T^6 (273.15 K<T<413.15K)

[1]Manufacturer's data sheet (Element 6 Ltd.)
[2]Manufacturer's data sheet (R. S. Components Ltd.)
[3]Manufacturer's data sheet (Gilbert Curry Ltd.)
[4]Expression taken from COMSOL 4.3b software

Table 2: Summary of boundary conditions used for the simulation of temperature at the diamond electrode/electrolyte interface

Boundary	Boundary type	Equation
1	Boundary heat source	$-\boldsymbol{n}\cdot(-\kappa\nabla T)=P_d$ $P_d=\frac{P}{A}$
2	Thermal insulation	$-\boldsymbol{n}\cdot(-\kappa\nabla T)=0$
3	Ambient temperature	293.15 °C
4	Axis of symmetry	$\nabla T\cdot\boldsymbol{n}=0$
5, 6	No slip fluid boundary	$\boldsymbol{v}=0$
5	Butler Volmer kinetics	$k_f=k^0e^{\frac{\alpha nF\left(E-(E^0+\beta\Delta T)\right)}{RT}}$ $k_b=k^0e^{\frac{(1-\alpha)nF\left(E-(E^0+\beta\Delta T)\right)}{RT}}$ $j_{elec}=k_fC_{ox,elec}-k_bC_{red,elec}$